Quart. J. R. Met. Soc. (1976), **102**, pp. 791–804

551.515.31 : 551.558.1

Thermally driven vortices: a numerical study with application to dust-devil dynamics

By R. K. SMITH and L. M. LESLIE

Department of Mathematics, Monash University, Clayton, Australia, 3168

Australian Numerical Meteorology Research Centre, P.O. Box 5089AA, Melbourne, Australia, 3001

(Received 31 October 1975, revised 12 March 1976)

SUMMARY

This paper describes a series of numerical experiments designed to explore the close interplay between the rotational, the pressure gradient, and the buoyancy, force fields in concentrated vortex flows driven thermally by heating from below. The calculations are motivated by a desire to understand the dynamics of dust-devils and to provide a theoretical framework in terms of which both past and future observations of these vortices may be interpreted.

In the model, a vortex is generated along the vertical axis of a cylindrical region of fluid bounded by a rigid (no-slip) lower boundary, and a sidewall consisting of a rigid, impermeable upper portion and a rotating, porous, lower portion through which fluid at ambient temperature enters the cylinder and acquires rotation. The flow is driven by maintaining a circular portion of the lower boundary at a fixed temperature above ambient and fluid is allowed to enter or leave the cylinder normally through the upper boundary. For a cylinder of given size, the flow behaviour depends on the magnitudes of two nondimensional parameters which characterize the strength of the thermal forcing and of the imposed rotation. According to the sizes of these, flows with axial downflow on part or all of the axis of rotation are possible and, in some cases, a closed cell of reversed flow is possible. In each case it is possible to give a complete description of the force field balance which combines to produce the particular flow pattern.

The calculations go a long way to providing an understanding of the main features of dust-devils as observed in a careful and detailed study by Sinclair and corroborate well with the experimental results of Fitzgarrald in relation to laboratory vortices. In particular, we show how rotationally induced axial pressure gradients can supplement buoyancy forces in accelerating the vertical flow in dust-devils as appears necessary to explain the large vertical accelerations observed near the ground in these vortices.

1. INTRODUCTION

Numerical models continue to play a central role in studies of vortex dynamics; a field in which analytical techniques have proved to be severely limited, and laboratory experiments and observational programmes have been restricted, either by difficulties in measuring the fully three-dimensional flow field patterns, the interpretation of flow visualization, or simply access as in the case of naturally occurring vortices such as dust-devils, waterspouts and tornadoes. Numerical studies, in contrast, can provide complete information on the patterns of flow and force fields which occur in vortices during all stages of their lifetimes. Information in such detail is essential to enable one to unravel the intimate coupling which is known to exist between the axial and azimuthal flow fields of a vortex; a coupling which is greatly augmented by the presence of a non-yielding boundary normal to a vortex core.

In this paper we present the results of some numerical experiments with thermally driven vortices with the particular view to understanding the mechanics of dust-devils; a broad range of atmospheric vortices which occur on hot days over dry terrain.

Although the more intense dust-devils occur predominantly in the desert regions of the world and particularly in the summer months when insolation is at a maximum, weaker types occur in other areas, even in the temperate latitudes, on hot summer days. There

is little doubt that these vortices are generated by the amplification of locally enhanced sources of ambient vorticity by thermals resulting from strong ground heating. As the name implies, those dust-devils which can be seen are made visible by dust particles or other debris which are picked up at the ground and carried aloft in the thermal current, but it is likely that in many cases suitable visualization particles are absent, for example, Businger has inferred the presence of these vortices from tuft patterns produced over a wheat field (see Morton 1966), and dust-devils may be more common than is generally realized. Moreover, it is quite possible that they play an important role in the transfer of heat and momentum in the lower layers of the atmosphere in conditions where lapse rates are highly super-adiabatic.

As a result of extensive observational programmes conducted in the desert regions of Arizona (Sinclair 1964, 1965, 1969, 1973) and in the Mojave Desert (Ryan and Carroll 1970; Carroll and Ryan 1970; Ryan 1972) valuable data on dust-devils have been collected and these, together with some measurements by Kaimel and Businger (1970), have enabled the principal features of these vortices to be identified, at least in their lowest levels. At the same time the observations raise a number of questions which we shall consider later. In view of the erudite account of earlier observational studies (including preliminary measurements made by Sinclair 1964, 1965) and of other aspects of dust-devils contained in the review article by Morton (1966), only a brief description is needed here.

Dust-devils range considerably in size, from a metre or so in diameter and height to tens of metres in diameter and several hundred metres in visible height, but thermals apparently associated with dust-devils have been identified by glider pilots at heights up to 4 km (Sinclair 1964). Maximum swirling velocities are typically of order $10\,\mathrm{m\,s^{-1}}$ and, although there are a few anomalous results, the majority of census studies indicate that the sense of rotation is random, as one would expect from scale considerations (see Morton p. 151 and Carroll and Ryan). Maximum vertical velocities are comparable with maximum swirling velocities (consistent with the predictions of Morton p. 178, based on an order of magnitude analysis of vortex core motions) and are usually attained quite close to the ground, often within a metre or two of it, but both Kaimel and Businger and Sinclair (1973) note that buoyancy forces alone cannot account for such large vertical accelerations. (Buoyancy force is defined relative to the local ambient temperature in the usual manner.) In that case, dynamic pressure gradients must assume an important role in driving the flow, but it is known that these are intimately connected with the swirling flow field and calculations are necessary to determine their contribution to the dynamics. In addition to furnishing such information, we believe our calculations also provide a framework for understanding the observations of vertical flow structure. In many cases these indicate the existence of a central core with downflow along the axis; in other cases there is considerably reduced upflow along the axis, possibly with downflow at greater heights, and flow stagnation at some point on the axis. In all cases the central core is surrounded by a region of vigorous upflow and swirl. Temperature data exhibit a warm core structure with maximum temperatures typically 3·5 to 5 K above ambient at heights of about 2 m, and 2 to 4 K in the height range 5 to 10 m. In some cases the warm air near the dust-devil centre is in the mean of order 0·5 to 1·0 K cooler than the surrounding core (Sinclair 1973). The above summary is based primarily on measurements made in the lower levels of dust-devils; below 9·5 m in the case of Sinclair's data and below 22·5 m in the observation reported by Kaimel and Businger. Measurements of flow fields at greater heights are not available but Ryan and Carroll (1970) have obtained temperature data at higher levels using an aircraft.

Theoretical studies of dust-devil type vortices have been made by Barcilon (1967) and Logan (1971) although both these analyses are limited in application and neither give information concerning core structure. Barcilon employs a momentum integral technique to represent the core flow and uses an entrainment assumption to relate the mean inflow at

a given height to the mean vertical velocity at that height, as in non-rotating plume models (Morton *et al.* 1956). However, the entrainment constant has not been determined for swirling flows, and furthermore it is questionable whether such a formulation is applicable when significant swirl is present, as this greatly inhibits the entrainment. Under these circumstances it is not even clear to what degree the mean vertical velocity is relevant. Logan assumes a given profile of azimuthal velocity above the terminating ground boundary layer of the vortex and uses a momentum integral technique to calculate the boundary layer flow and, in particular, the radial distribution of vertical flow just above the boundary layer, compatible with the specified profile of swirl. The method relies, amongst other things, on a suitable formulation for the boundary layer at large radial distances and in the case of 'long-thin' vortices such as dust-devils, waterspouts and tornadoes, the flow at radial distances greater than a few core diameters is not well known but almost certainly has the character of flow towards a sink, rather than a shallow, viscous layer exhibiting gradual radial development. Indeed, this even seems to be the case in certain contained vortices as suggested by the numerical study of boundary effects in vortex flows by Bode *et al.* (1975). Thus it is difficult to determine the extent to which Logan's formulation is appropriate.

Thermally driven vortices have also been studied in the laboratory and some of the findings are pertinent to dust-devils and to the present calculations. Emmons and Ying (1967) use a pool of acetone, burning in air, as a heat source and rotation is supplied by a rotating screen with its axis vertical and centred above the pool. In this arrangement, air which converges in low levels towards the fire acquires angular momentum as it enters the screen. Since angular momentum is approximately conserved (there is a small frictional loss due to the torque at the lower boundary), the azimuthal velocity of the air increases with decreasing radius and a vortex is formed as this swirling air is convected into the plume above the fire. Measurements are made of temperature profiles across the vortex, of the radial spread with height and of the acetone burning rate, for a range of screen rotation rates. One of the principal findings is that turbulent mixing is suppressed in the core as the rotational motion increases in strength and this reduced mixing can deprive the fuel vapour of oxygen needed for combustion to such an extent as to substantially increase the height of the acetone flame. Barcilon uses the same apparatus as Emmons and Ying but instead of the pool fire he situates a heated plate over most of the lower boundary to provide the field of buoyancy. Flow visualization is achieved by a small smoke generator located on the lower boundary at the screen axis. Barcilon gives a brief description of the visual behaviour of the vortex as the screen rotation rate is increased, but does not give any quantitative measurements of the flow fields. A more comprehensive series of laboratory experiments are reported by Fitzgarrald (1973) and again the working fluid used is air. Buoyancy is also produced by heating the lower boundary but swirl is imparted to inflowing air by a series of vanes situated around the perimeter of the radial boundary. Two angular settings of the vanes were available allowing a change in imposed swirl strength for a given plate temperature but in this arrangement it is not possible in general to vary the plate temperature and imposed swirl strength independently. However, Fitzgarrald found that flow visualization and optical velocity measurements were much simpler in this configuration. Data are presented for a range of plate temperatures and hence inflow angles (for a given vane setting the swirl strength increases with the radial inflow speed which in turn is an increasing function of plate temperature: Fitzgarrald defines inflow angle as the inverse tangent of mean azimuthal velocity divided by mean inflow velocity at the vane radius where averages are taken over the lowest one-third of the apparatus height and over eight-minute intervals) and five parameter regimes are identified according to the strength of rotation for a given plate temperature. For small inflow angles, and hence small rotation rates, no significant vortex occurs. As the rotation rate is increased, a one-cell vortex is observed; there is no stagnation

point on the axis and the flow is upwards at any radius. A further increase in rotation rate results in a two-cell vortex with a much stronger circulation and the motion on the axis is either positive and very small, or slightly negative. Vortex breakdown is common in these situations. A continued increase in rotation results in a strong two-cell vortex with substantial axial downflow and ultimately, when the rotation is very large, the flow becomes one of solid body rotation with an extensive region of downflow at the centre and no concentrated vortex is formed. The present calculations are in concordance with these results.

2. THE MODEL

The numerical model combines various features of the laboratory simulations described above and corresponds broadly with an experimentally realizable situation. It is portrayed in Fig. 1. The computational region is cylindrical with radius R and depth H and has its

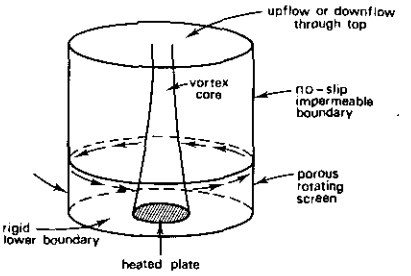

Figure 1. Sketch of flow configuration in the model.

axis vertical. It is bounded by a rigid (no-slip) lower boundary and a sidewall consisting of an insulated, rigid, impermeable upper portion together with a rotating, porous, lower portion with depth h through which fluid with ambient temperature T_e may enter the cylinder, acquiring rotation as it does so. The flow is assumed to be axisymmetric and is driven by maintaining a circular portion of the lower boundary, with radius R_s, at a fixed temperature T_s, higher than T_e. Fluid is allowed to enter or leave the region normally through the upper boundary and it is assumed that advection of heat dominates transfer due to diffusion at this level.

The fluid has density ρ and temperature T and the diffusivities of momentum and heat, K_M and K_H, are taken to be constant and in most of the calculations are taken to be equal. In certain parameter regimes, and depending on the physical characteristics of the working fluid, the flow may be either laminar or turbulent. In our calculations we explore a range of parameters as close as possible to the conditions of Barcilon's experiments and with values for turbulent diffusivities chosen as representatively as possible. We also assume air as the working fluid.

The equations of momentum (assuming the Boussinesq approximation is valid), heat, continuity and state are,

$$\frac{D\mathbf{u}}{Dt} = -\frac{1}{\rho_e}\nabla p + \frac{T - T_e}{T_e}\mathbf{g} + K_M\nabla^2\mathbf{u} \quad . \quad . \quad (1)$$

$$\frac{DT}{Dt} = K_H\nabla^2 T \quad . \quad . \quad . \quad . \quad . \quad (2)$$

$$\nabla\cdot\mathbf{u} = 0 \quad . \quad . \quad . \quad . \quad . \quad . \quad (3)$$

and

$$\rho T = \rho_e T_e \quad . \quad . \quad . \quad . \quad . \quad . \quad (4)$$

where $\mathbf{u} = (u, v, w)$ is the velocity referred to a cylindrical coordinate system (r, θ, z), coaxial with the computational region, $\mathbf{g} = (0, 0, -g)$ is the gravitational acceleration, p is the dynamic pressure and ρ_e is the ambient density, assumed uniform. The computational domain is the region $0 \leqslant r \leqslant R$; $0 \leqslant \theta < 2\pi$; $0 \leqslant z \leqslant H$. Axial symmetry, $\partial/\partial\theta \equiv 0$, is assumed.

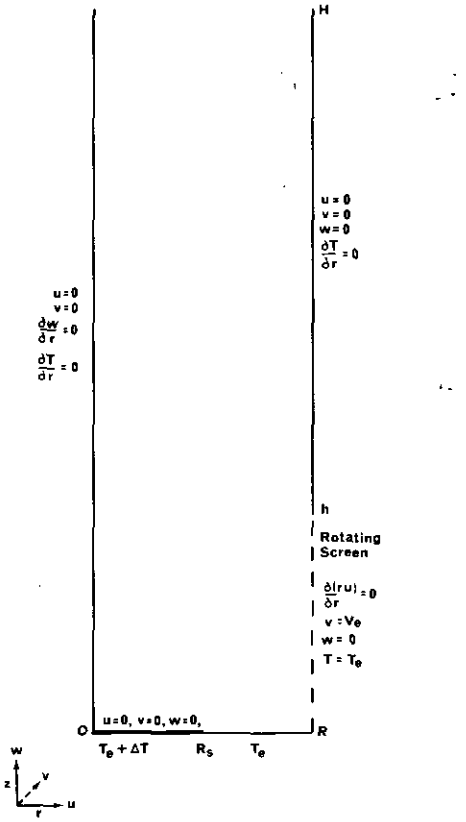

Figure 2. Schematic representation of the boundary conditions used in the calculations.

The boundary conditions conforming with the description given above are displayed in Fig. 2; they are as follows:

$$\text{On } z = 0: \qquad u = 0, \quad v = 0, \quad w = 0, \quad T = \begin{cases} T_s (= T_e + \Delta T): & 0 \leqslant r \leqslant R_s, \\ T_e & : R_s < r \leqslant R, \end{cases}$$

$$\text{On } z = H: \qquad u = 0, \quad \partial v/\partial z = 0, \quad \partial w/\partial z = 0, \quad \partial T/\partial z = 0,$$

$$\text{On } r = 0: \qquad u = 0, \quad v = 0, \quad \partial w/\partial r = 0, \quad \partial T/\partial r = 0,$$

$$\text{On } r = R: \qquad \begin{cases} \text{for } 0 \leqslant z < h: & \partial(ur)/\partial r = 0, \quad v = V_e, \quad w = 0, \quad T = T_e, \\ \text{for } & h \leqslant z \leqslant H: \; u = 0, \quad v = 0, \quad w = 0, \quad \partial T/\partial r = 0. \end{cases}$$

These conditions are not all independent.

The principal nondimensional flow parameters are, a pseudo-Rayleigh number:

$$Ra = g \frac{\Delta T}{T_e} \frac{R_s^3}{K_M^2},$$

which characterizes the strength of buoyancy forces compared with viscous forces, and a swirl parameter:

$$Rt = \frac{V_e R}{R_s}\left[g\frac{\Delta T}{T_e}R_s\right]^{-\frac{1}{2}},$$

which is a measure of the rotational constraint for a given level of thermal forcing and a given source radius (*N.B.* In this definition we have used a swirling velocity scale V_eR/R_s appropriate to the source radius, obtained on the hypothetical assumption of angular momentum conservation in the low level inflow).

The other parameters include a pseudo Prandtl number $Pr = K_M/K_H$ (which is simply equal to the Prandtl number in the usual sense if the flow is laminar), and three aspect ratios: $A_1 = h/H$, $A_2 = R/H$, $A_3 = R_s/R$. Our primary goal is to explore the types of flow which occur for different values of Ra and Rt, keeping other parameters fixed. However, some experimentation involving changes of one of K_M, H, h, keeping all other quantities fixed, contributes to a fuller understanding of the vortex dynamics and helps one to assess the relevance of the model to other vortex flows, in particular dust-devils.

The details of the numerical method of solution, which is very similar to that used by Leslie (1971), are given briefly in an appendix. In short, the equations of motion and boundary conditions given above are reduced to a form suitable for numerical integration and the calculations are started with the flow in an initially quiescent state at ambient temperature. The heat source and rotating screen are 'switched on' at the initial instant and the integrations are carried out until a steady state is attained. The results we describe relate entirely to the steady-state fields.

3. Parameter values for the experiments

For definiteness, we base our selection of the flow parameters broadly on the laboratory experiments of Barcilon (1967) and Fitzgarrald (1973) in which air is the working fluid. Thus, for the two principal experiments, 1 and 2, the flow is defined by the values: $H = 100\,\text{cm}$, $R = 30\,\text{cm}$, $R_s = 15\,\text{cm}$, $\Delta T = 20\,\text{K}$ or $30\,\text{K}$, $T_e = 300\,\text{K}$, $V_e = 1{\cdot}57\,\text{cm s}^{-1}$ (equivalent to half a screen revolution per minute) and K_M, $K_H = 1{\cdot}5\,\text{cm}^2\text{s}^{-1}$. Obviously, if one's intention is to compare an *actual* laboratory experiment with the corresponding calculation, the values chosen for K_M and K_H (which are arbitrarily taken to be about 15 times the molecular viscosity for air at room temperature) are arguable although they are probably reasonable to an order of magnitude. However, this ever-present difficulty of choosing appropriate values for turbulent diffusivities in 'K-formulations' need not concern us unduly here, since precise values are not immediately relevant to the type of information we seek from the calculations (see section 4). Subsidiary experiments 3 to 6, based on experiment 1 with one change, are also discussed; the changes being respectively: a doubling

TABLE 1

Experiment	1	2	3	4	5	6
ΔT(K)	20	30	20	20	20	20
V_e(cm s^{-1})	1·57	1·57	3·14	1·57	1·57	1·57
Ra	$\sim 10^5$	$\sim \frac{3}{2} \times 10^5$	$\sim 10^5$	$\sim 10^5$	$\sim 10^5$	$\sim 10^5$
Rt	0·10	0·08	0·20	0·10	0·10	0·10
Pr	1	1	1	0·5	1	1
A_1	0·3	0·3	0·3	0·3	0·15	0·3
A_2	0·3	0·3	0·3	0·3	0·3	0·2
A	58	83	41	61	64	58

of Ω, the angular velocity of the screen; a halving of K_M; a halving of h; and an increase of H by 50%.

The parameter values for the six experiments are listed in Table 1. Also listed in this table are values for the derived quantity $A = \dfrac{v_{max}/r_{max}}{V_e/R}$, which is a measure of the amplification of the imposed rotation. In this expression, v_{max} is the maximum swirling velocity attained in the flow and r_{max} is the radius at which this occurs. The results are discussed below.

4. Discussion

An essential feature of all the flows studied is a region of warm air above the source which gives rise to a locally reduced pressure along the axis and (unless the screen rotates too rapidly) draws fluid inwards through the screen. As a ring of fluid converges towards the axis, it approximately conserves its angular momentum (unless viscous forces are everywhere predominant) and spins faster. Thus the centrifugal force it experiences increases. As is well known (see e.g. Morton) a concentrated vortex will form only if, *for a given heating strength,* the angular velocity Ω lies within a certain range of values. If Ω is too small, centrifugal forces never exceed a small fraction of the local radial pressure gradient and the flow has essentially the character of a thermal plume, modified only slightly by rotation. However, if Ω is very large, inflowing fluid may travel only a small radial distance before the centrifugal force is sufficient to balance the radial pressure gradient, or in the extreme case, balance may be impossible and the screen then acts as a centrifugal pump. For a range of intermediate values of Ω, approximate balance between radial forces is attained at small radii; rings of fluid then attain large rates of rotation compared with that of the screen and are advected with the vertical flow to form a concentrated vortex core. The close balance between radial forces permits only weak radial motion along most of the core, but adjacent to the lower boundary centrifugal forces are substantially reduced by frictional effects leaving a net inwards pressure gradient. Thus most of the radial mass flux occurs in a shallow friction layer at the base of the vortex. Moreover, the radial distribution of this flux, and hence by continuity the radial distribution of vertical motion just above the friction layer, is determined by the radial profile of azimuthal velocity at this level. In certain cases the radial inflow may be completely expelled as upflow at a finite distance from the axis: these cases correspond with two-celled vortices having downflow on the entire axis.

Clearly the boundary layer dynamics exerts a strong constraint on the vortex structure by providing a coupling between the azimuthal and axial flow fields at low levels. But this is not the only coupling between these two flow fields as can be seen as follows. Above the boundary layer, the equation expressing approximate radial force balance may be integrated across the vortex to give

$$p(R, z) - p(0, z) = \rho \int_0^R (v^2/r)\, dr. \qquad (5)$$

If $p(R, z)$ is appreciably uniform, as is the case over most of the flow excluding the source region (see Fig. 3), we see that a change in the azimuthal velocity $v(r, z)$ with height is associated in general with an axial pressure gradient. Indeed, if the swirling velocity decreases with height and/or if the profile spreads out so that the larger velocities are displaced to larger radii, an *adverse* axial pressure gradient is induced. On the other hand, if the swirling flow increases with height, as it must do just above the ground, a *favourable* axial pressure gradient tendency occurs. This coupling plays a central role in vortex dynamics

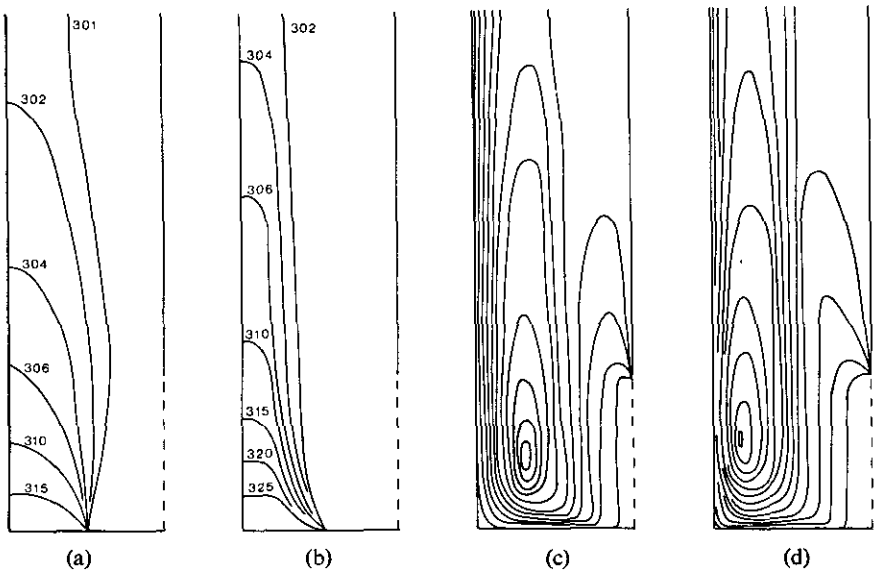

Figure 3. Comparison of steady state isotherms and isotachs of swirling velocity in experiments 1 and 2: (a) isotherms, $\Delta T = 20\,\mathrm{K}$; (b) isotherms, $\Delta T = 30\,\mathrm{K}$; (c) v isotachs, $\Delta T = 20\,\mathrm{K}$; (d) v isotachs, $\Delta T = 30\,\mathrm{K}$.

and provides a basis for understanding not only the range of flows which occur in our calculations, but also many of the observations on laboratory and atmospheric vortices, including dust-devils.

The above ideas are not new and are discussed by Morton, although their significance does not seem to be widely appreciated in the literature. It is particularly interesting to see how they relate to thermally driven vortices, and that is one of the purposes of our study. The interplay between buoyancy forces and axially induced pressure fields is brought out

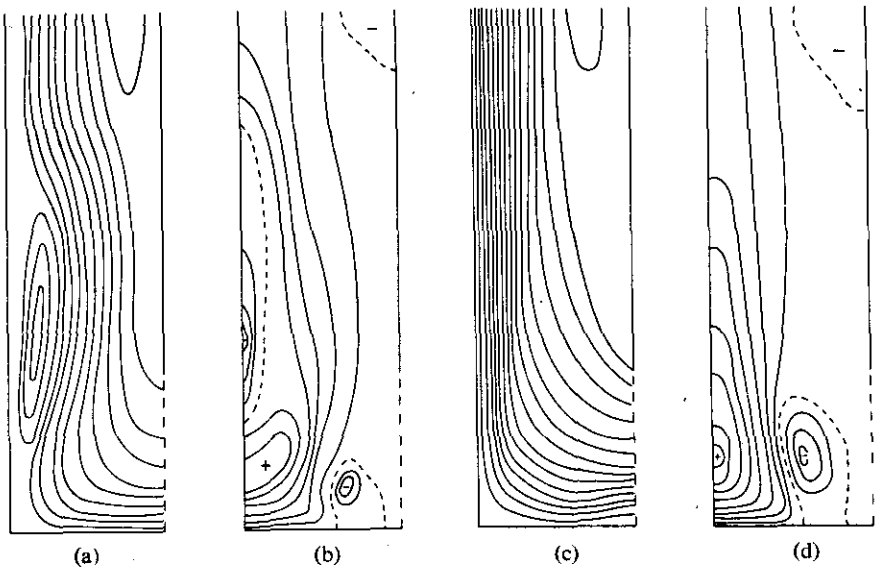

Figure 4. Comparison of steady state streamline patterns and contours of vertical force in experiments 1 and 2:
(a) streamlines, $\Delta T = 20\,\mathrm{K}$; (b) iso-$F$ curves, $\Delta T = 20\,\mathrm{K}$;
(c) streamlines, $\Delta T = 30\,\mathrm{K}$; (d) iso-$F$ curves, $\Delta T = 30\,\mathrm{K}$

clearly in a comparison between experiments 1 and 2 (see Figs. 3–5) which both exemplify a concentrated vortex flow (cf. values of A in Table 1).

Fig. 3 compares the isotherms and swirling velocity fields for the two experiments and shows that with stronger forcing ($\Delta T = 30$ K) a narrower vortex is formed. This is consistent with a radial force balance being attained at smaller radii, as discussed above. In each case the core radius, characterized by the radius of maximum swirl, decreases rapidly with height at first and the swirl intensifies. The intensity stabilizes at a minimum core radius and thereafter it lessens, accompanied by a gradual spread of the vortex. A similar radial expansion occurs in dust devils at heights above 2 m (Sinclair 1973, p. 1609). Although the patterns of isotherms and azimuthal isotachs are broadly similar, the meridional flow patterns differ substantially (Fig. 4). At the stronger forcing level ($\Delta T = 30$ K), the flow is upwards along the whole vortex core, with a weak downflow near the sidewall, presumably induced by the presence of the sidewall itself. However, for weaker forcing ($\Delta T = 20$ K), there is a closed cell of circulation with downflow adjacent to the axis, where the adverse vertical pressure gradient is larger than the buoyancy force. This can be seen in Fig. 4(b) which shows contours of equal vertical force (dynamic pressure gradient + buoyancy force), henceforth referred to as iso-F curves, where

$$F = -\frac{1}{\rho_e}\frac{\partial p}{\partial z} + g\left(\frac{T - T_e}{T_e}\right). \qquad (6)$$

The corresponding iso-F curves for $\Delta T = 30$ K are also consistent with the meridional streamline pattern obtained in that case. Note that even in the absence of rotation, dynamic pressure gradients (as commonly defined herein and elsewhere) may not be ignored in significant regions of the flow (Smith *et al.* 1975). For example, just above the heat source, $Dw/Dt \approx 0$ whence from the z-component of Eq. (1), we have

$$\frac{1}{\rho_e}\frac{\partial p}{\partial z} \approx g\left(\frac{T_s - T_e}{T_e}\right) + K_M \left.\frac{\partial^2 w}{\partial z^2}\right|_{z=0}.$$

At high pseudo-Rayleigh numbers, the viscous term may be neglected in this equation and the dynamic pressure gradient approximately balances the buoyancy force. This is a consequence of the definition of the dynamic pressure p as the deviation from the ambient hydrostatic pressure, and the corresponding definition of buoyancy force. It is also consistent with the fact that immediately above the source, the local horizontal temperature gradient, and hence the local buoyancy force (essentially F in the case of zero rotation) is small.

We conclude that in the absence of rotation, dynamic pressure gradients in a region immediately above the source have their z-component directed downwards to compensate for the over-estimate in forces due to buoyancy given by the formula $g(T-T_e)/T_e$. Above one or two source diameters in height, it turns out that $F \approx g(T-T_e)/T_e$ and $-\rho_e^{-1}\partial p/\partial z \approx 0$, except in the vicinity of an inversion (see Smith *et al.* for a fuller discussion). When rotation is present, and at heights where the swirling velocity field is spreading and decaying, we also expect dynamically induced pressure gradients with downward components. However, below the height of maximum swirl where the vortex narrows with height, it seems possible that an upwards pressure gradient could be induced by rotation and this might be comparable with or exceed the buoyancy force. Since F must be small just above the source, the upwards pressure gradient could not be positive at the boundary itself or in a (possibly shallow) layer immediately above it.

It seems to us necessary to invoke this effect to account for the large vertical accelerations in dust devils close to the ground as observed by Sinclair (1973) and Kaimel and Businger (1970) as no vertical driving forces other than pressure gradient and buoyancy

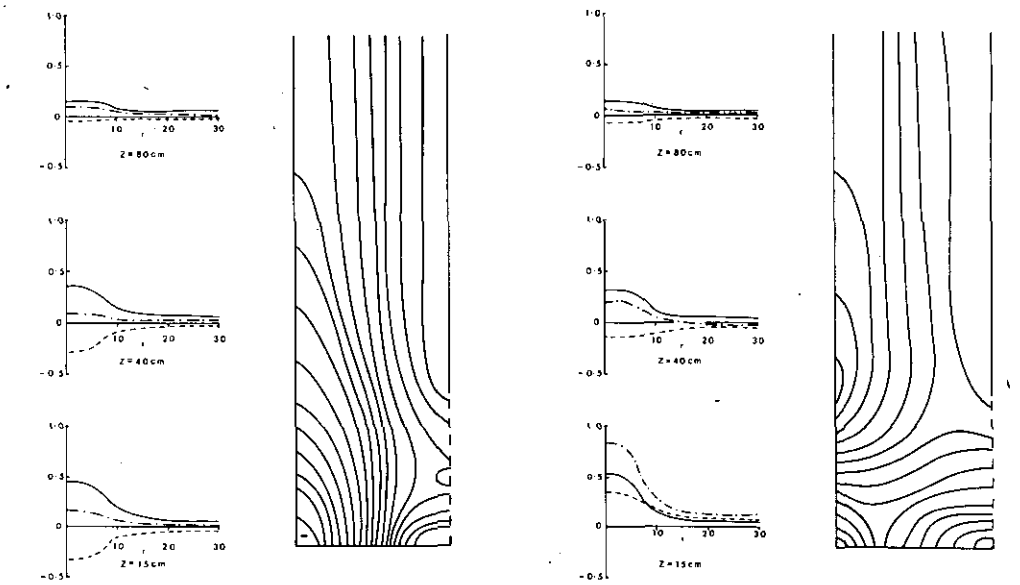

Figure 5. Comparison of steady state isobars and radial profiles of $-\varrho_e^{-1}\partial p/\partial y$, dashed curves; $g(T-T_e)/T_e$, solid curves; and $F = -\varrho_e^{-1}\partial p/\partial y + g(T-T_e)/T_e$, dot-dashed curves; at selected heights in experiments 1 and 2: (a) comparison of vertical force profiles, $\Delta T = 20\,\mathrm{K}$; (b) isobars, $\Delta T = 20\,\mathrm{K}$; (c) comparison of vertical force profiles, $\Delta T = 30\,\mathrm{K}$; (d) isobars, $\Delta T = 30\,\mathrm{K}$. Note in (c) and (d) there is a height range in which the rotationally induced vertical pressure gradient is comparable with, and in the same direction as, the buoyancy force.

force $g(T-T_e)/T_e$, can be envisaged. That such an effect does occur, but not always, is demonstrated in Fig. 5 which shows the isobars in experiments 1 and 2 and compares the radial profiles of $\rho_e^{-1}\partial p/\partial z$, $g(T-T_e)/T_e$ and F at selected heights in these two flows. In the case $\Delta T = 20\,\mathrm{K}$, the dynamic pressure gradient is negative over the entire vortex core. Hence, even at low levels, the rapid increase in swirl with height (Fig. 3(c)) is insufficient to induce a net favourable pressure gradient along the axis. However, for stronger forcing ($\Delta T = 30\,\mathrm{K}$) the tighter and stronger swirling flow field is able to induce a favourable axial pressure gradient, comparable in magnitude with, but in this case slightly smaller than, the buoyancy force $g(T-T_e)/T_e$. Sinclair (1973, p. 1607) notes that typical dust-devil measurements indicate vertical accelerations near the ground of order $5\,\mathrm{m\,s^{-2}}$ which if produced by buoyancy forces $g(T-T_e)/T_e$ alone would require $\Delta T \approx 150\,\mathrm{K}$ for $T_e \approx 300\,\mathrm{K}$. Such large horizontal temperature differences are not possible. Sinclair concludes that the dynamic pressure gradients must therefore be important but does not suggest how these might arise. We have not studied a wide range of parameter values to date, primarily because the fine-mesh resolution and small timestep used for integrating the equations make the calculations expensive in computer time (see appendix for details). Nevertheless, it seems reasonable to believe that parameter regimes exist in which upwards pressure gradients are several times as large as $g(T-T_e)/T_e$ in the lower part of the vortex, values which would be required to corroborate quantitatively with the measurements in dust-devils.

Fig. 6 shows profiles of vertical velocity at two selected heights for the case $\Delta T = 30\,\mathrm{K}$. At the lower height ($z = 15\,\mathrm{cm}$) the maximum vertical velocity occurs at the axis but higher up ($z = 40\,\mathrm{cm}$) the maximum is displaced radially and there is a local minimum at the axis. Sinclair (1973, p. 1608) observes profiles of the latter type at 2 m and in one case at 9·5 m above the ground in dust devils and explains this effect as being possibly "... due to the 'pinching-off' of the descending core by the radial field of motion at some higher

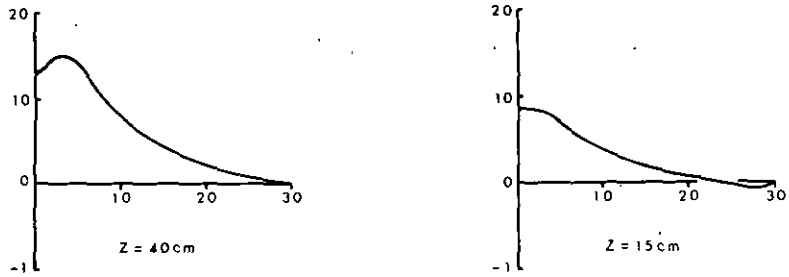

Figure 6. Vertical velocity profiles at heights $z = 15\,\text{cm}$ and $z = 40\,\text{cm}$ in experiment 2 ($\Delta T = 30\,\text{K}$).

elevation". The present calculations show that it is due to the reduced value of F at the axis which in turn results from the downwards pressure gradient induced by axial decay and radial spread of the swirling flow with height as discussed above: see also Fig. 5(c) and note in particular the local minimum of $\rho_e^{-1}\partial p/\partial z$ at $r = 0$, a feature which is absent in the profile of $g(T-T_e)/T_e$.

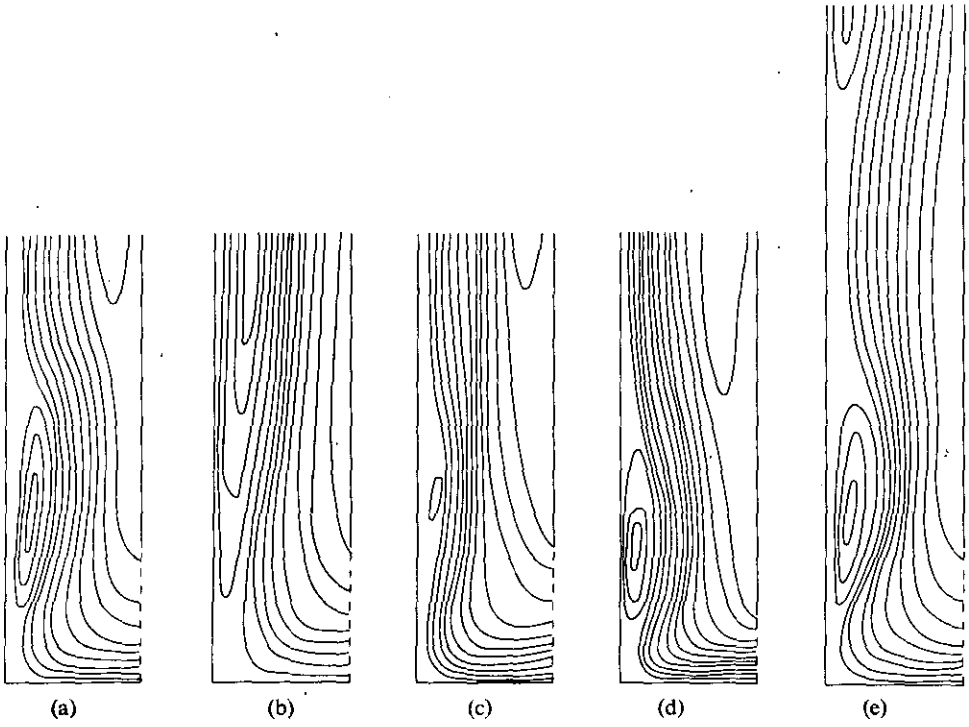

Figure 7. Comparison of streamfunction patterns between experiments 3–6 and experiment 1: (a) Expt. 1, the prototype; (b) Expt. 3, Ω doubled; (c) Expt. 4, K_M halved; (d) Expt. 5, inflow height halved; (e) Expt. 6, computational domain increased in height by 50%. For discussion see text.

The changes in flow behaviour as one of the quantities Ω, K_M, h, H are varied in turn from their values in experiment 1 are brought out in Fig. 7. This compares the meridional stream-function pattern in experiments 3 to 6 (Figs. 7(b)–7(e) respectively) with that in experiment 1 (Fig. 7(a)). The changes are consistent with expectations based on the foregoing discussion. Thus, doubling the screen rotation speed (Fig. 7(b)) increases the centrifugal force field on inflowing fluid and the centrifugal/radial pressure gradient force balance is attained earlier at a larger radius. Indeed, no inflowing fluid is able to penetrate to the centre

and the region of downflow extends along the entire axis, giving a broader, two-cell vortex. Halving the diffusivity of momentum K_M reduces the rate of decay of the swirling flow with height and therefore the induced adverse pressure gradient along and adjacent to the axis. In consequence, the reversed cell is much weaker (Fig. 7(c)). Halving the inflow height h produces a slightly more intense vortex with a slightly smaller reversed cell of circulation (Fig. 7(d)). Apparently the increased inertia of inflowing fluid is sufficient to reduce slightly the radius at which radial force balance is attained. Finally, increasing H by 50% produces little change in the flow pattern below $z = 1$ m (Fig. 7(e)), confirming the choice of boundary conditions at the upper boundary as ones which create little unintended constraint on free flow through that boundary. Just below $z = 1{\cdot}5$ m there is a further axial stagnation point with downflow above. Again this is a feature which one expects due to the continued decay and radial spread of the swirling flow with height, coupled with a continued reduction of the buyoyancy field along the core, due principally to the lateral diffusion of heat.

It would appear that axial downflow is a prevalent feature of convectively driven vortices of the 'tall-thin' variety, although if buoyancy forces are sufficiently strong, downflow may be confined to upper levels. This explains why there is some variability in Sinclair's measurements of vertical flow in dust-devils; recall that in some cases, downflow was observed only at the larger probe height. Sinclair (1973 p. 1606) also notes the presence of slightly cooler air within the warm central core of dust-devils, being in the mean $\sim 0{\cdot}5$–$1{\cdot}0$ K cooler than the surrounding core. As noted by Sinclair (p. 1608), this may be simply due to the downwards advection of air from altitudes at which mixing with ambient air is further advanced. In view of this temperature anomaly, one might suspect the validity of the temperature condition $\partial T/\partial z = 0$ at $z = H$, chosen in our model. If there is descending air in the central core, and if this is slightly cooler than the ascending air in the outer core, it might seem more appropriate to prescribe $T(r, H)$ at radii where $w(r, H) < 0$. But unless measured data from an actual laboratory experiment are available, one has no means of choosing a realistic temperature distribution for the descending air at $z = H$ as this depends in an unknown way on the subsequent development and thermal structure of the ascending air above $z = H$. Further, the condition $\partial T/\partial z|_{z=H} = 0$ as used herein does allow the temperature distribution in the descending air to be influenced by that of the ascending air and although neither condition is strictly correct, the one we have used appears to be very satisfactory. In the present experiments we did not detect local temperature minima in upper level downflows but there seems little reason why these could not occur in some parameter regimes.

The dependence of vortex behaviour on the principal flow parameters as determined herein corresponds closely with the experimental results of Fitzgarrald (see section 1), although it is not possible to make quantitative comparisons; primarily since representative values for turbulent diffusivities are not available for the experiments but also because of slight differences in the flow arrangement. Of course, in reality we must expect significant variations in eddy diffusivity between different regions of the flow; thus mixing will be suppressed where the local swirling field is stably stratified, $\partial(vr)/\partial r > 0$, and enhanced where it is unstably stratified, $\partial(vr)/\partial r < 0$ or where there are appreciable horizontal temperature gradients. Even so, it is unlikely that variations in K_M and K_H give rise to major structural changes in the flow. One feature of Fitzgarrald's observations which is not reproduced in our calculations is that of vortex breakdown in which the vortex core undergoes a sudden jump in radius, analogous to the sudden jump in water level at a hydraulic jump. Again, the failure of our numerical model to exhibit this phenomenon is probably related to our choice of constant eddy diffusivities and their particular values.

We have carefully resisted any claim to model a dust-devil with close realism but the model does contain the essential ingredients which are believed to lead to dust-devils, i.e.

strong thermal forcing from below in the presence of rotation. We are fully aware that our choice of boundary conditions at $r = R$, and possibly to a much lesser extent at $z = H$ (see above), impose constraints which are not present in the atmosphere but note that the physical interpretations of vortex behaviour described above are quite general and do not depend crucially on the particular model we have chosen to illustrate them. In view of this, there appears little reason to suspect their broad applicability to dust devils although this in no way means that *all* aspects of dust-devil behaviour, especially, for example, the flow at large heights, can be explained by resort to this particular model.

References

Barcilon, A. 1967 A theoretical and experimental model for a dust devil, *J. Atmos. Sci.*, **24**, pp. 453–466.

Bode, L., Leslie, L. M. and Smith, R. K. 1975 A numerical study of boundary effects on concentrated vortices with application to tornadoes and waterspouts, *Quart. J. R. Met. Soc.*, **101**, pp. 313–324.

Carroll, J. J. and Ryan, J. A. 1970 Atmospheric vorticity and dust devil rotation, *J. Geophys. Res.*, **75**, pp. 5179–5184.

Emmons, H. W. and Ying, S. J. 1967 The fire whirl, *Proceedings Eleventh Symposium on Combustion*, The Combustion Institute, pp. 475–488.

Fitzgarrald, D. E. 1973 A laboratory simulation of convective vortices, *J. Atmos. Sci.*, **30**, pp. 894–902.

Kaimel, J. C. and Businger, J. A. 1970 Case studies of a convective plume and a dust devil, *J. Appl. Met.*, **9**, pp. 612–620.

Leslie, L. M. 1971 The development of concentrated vortices: a numerical study, *J. Fluid Mec.*, **48**, pp. 1–21.

Logan, S. E. 1971 An approach to the dust devil vortex, *AIAA*, **9**, pp. 660–665.

Morton, B. R., Taylor, G. I. and Turner, J. S. 1956 Turbulent gravitational convection from maintained and instantaneous sources, *Proc. R. Soc., A*, **234**, pp. 1–22.

Morton, B. R. 1966 Geophysical vortices, *Prog. in Aeronautical Sci.*, **7**, pp. 145–194 (ed. Küchemann). Pergamon.

Ryan, J. A. 1972 Relation of dust devil frequency and diameter to atmospheric temperature, *J. Geophys. Res.*, **77**, pp. 7133–7137.

Ryan, J. A. and Carroll, J. J. 1970 Dust devil wind velocities: mature state, *Ibid.*, **75**, pp. 531–541.

Sinclair, P. C. 1964 Some preliminary dust devil measurements, *Mon. Weath. Rev.*, **92**, pp. 363–367.

1965 On the rotation of dust devils, *Bull. Amer. Met. Soc.*, **46**, pp. 388–391.

1969 General characteristics of dust devils, *J. Appl. Met.*, **8**, pp. 32–45.

1973 The lower structure of dust devils, *J. Atmos. Sci.*, **30**, pp. 1599–1619.

Smith, R. K., Morton, B. R. and Leslie, L. M. 1975 The role of dynamic pressure in generating fire wind, *J. Fluid Mech.*, **68**, pp. 1–19.

Appendix

Numerical method

The numerical method is very similar to that used by Leslie (1971) and need only be briefly described. Eqs. (1) to (3) are re-cast by introducing a stream function ψ, such that $u = -r^{-1}\partial\psi/\partial z$ and $w = r^{-1}\partial\psi/\partial r$, and the zonal vorticity component ζ, given by $\zeta = \partial u/\partial z - \partial w/\partial r$. In terms of ψ, ζ, v and T the finite-difference equations corresponding to Eqs. (1) to (3) are

$$\delta_t\overline{\zeta}^t + \mathrm{J}_A(\zeta/r) = \frac{1}{r}\delta_z(\overline{v^2}^z) + K_M\left\{\delta_{zz}\zeta + \delta_r\left[\frac{1}{r}\delta_r(r\zeta)\right]\right\}, \tag{A.1}$$

$$\delta_t \overline{v}^t + \frac{1}{r} J_A(v) = \frac{v}{r} \delta_z \overline{\psi}^z + K_M \left\{ \delta_{zz} v + \delta_r \left[\frac{1}{r} \delta_r (rv) \right] \right\}, \quad (A.2)$$

$$\delta_t \overline{T}^t + \frac{1}{r} J_A(T) = K_H \left\{ \delta_{zz} T + \delta_r \left[\frac{1}{r} \delta_r (rT) \right] \right\}, \quad (A.3)$$

$$\zeta = -\delta_r \left(\frac{1}{r} \delta_r \psi \right) - \frac{1}{r} \delta_{zz} \psi, \quad (A.4)$$

where $\overline{\theta}^x = \frac{1}{2}\left[\theta\left(x + \frac{\Delta x}{2}\right) + \theta\left(x - \frac{\Delta x}{2}\right) \right]$, $\theta_x = \frac{1}{\Delta x}\left[\theta\left(x + \frac{\Delta x}{2}\right) - \theta\left(x - \frac{\Delta x}{2}\right) \right]$,

and $J_A(\theta)$ is an Arakawa conserving finite-difference operator. The diffusion terms are to be evaluated at preceding time levels in order to avoid computational instability.

The boundary conditions now become:

At $r = 0$: $\zeta = \psi = v = \partial T/\partial r = 0$

At $z = 0$: $\zeta = -(1/r)(\partial^2\psi/\partial z^2)$, $\psi = \partial\psi/\partial z = v = 0$, $\begin{cases} T = T_e + \Delta T & 0 \leqslant r \leqslant R_s \\ T = T_e & R_s < r \leqslant R \end{cases}$

At $r = R$: for $0 \leqslant z \leqslant h$

$$\zeta = -\frac{\partial}{\partial r}\left(\frac{1}{r}\frac{\partial\psi}{\partial r}\right) - \frac{1}{r}\frac{\partial^2\psi}{\partial z^2}, \quad \frac{\partial\psi}{\partial r} = 0, \quad v = V_e, \quad T = T_e.$$

for $h \leqslant z \leqslant H$

$$\zeta = -\frac{\partial}{\partial r}\left(\frac{1}{r}\frac{\partial\psi}{\partial r}\right) - \frac{1}{r}\frac{\partial^2\psi}{\partial z^2}, \quad \frac{\partial\psi}{\partial r} = 0, \quad \frac{\partial\psi}{\partial z} = 0, \quad v = 0, \quad \frac{\partial T}{\partial r} = 0.$$

At $z = H$:

$$\zeta = -\frac{\partial}{\partial r}\left(\frac{1}{r}\frac{\partial\psi}{\partial z}\right) - \frac{1}{r}\frac{\partial^2\psi}{\partial z^2}, \quad \frac{\partial\psi}{\partial z} = \frac{\partial v}{\partial z} = \frac{\partial T}{\partial z} = 0.$$

The grid used for the numerical calculations consists of 101 points in the vertical and 31 points in the horizontal, which corresponds to a grid spacing of 1 cm. Approximately 6000 timesteps were required for each calculation, requiring roughly 5 hours computation time using the Australian Bureau of Meteorology IBM 360/65 computer.